Adhesive Hard-Sphere Colloidal Dispersions. A Small-Angle Neutron-Scattering Study of Stickiness and the Structure Factor

C. G. de Kruif,*[,†] P. W. Rouw,[†] W. J. Briels,[‡] M. H. G. Duits,[†] A. Vrij,[†] and R. P. May[§]

Van't Hoff Laboratory, University of Utrecht, Padualaan 8, De Uithof, 3584 CH Utrecht, The Netherlands

Small-angle neutron-scattering structure factor measurements were made on sterically stabilized silica spheres dispersed in benzene up to volume fractions of 0.30. Benzene is only a marginal solvent for the stabilizing layer on the surface of the particles. The particles are made attractive by lowering temperature. This attraction is modeled by a square well potential, the depth of which varies with temperature. At the highest temperature studied, our experimental system behaved effectively as an assembly of hard spheres, whereas at the lowest temperature the system approaches a spinodal. Using Baxter's theory we were able to evaluate the interaction parameters and to calculate the structure factor. Experimental structure factors were satisfactorily reproduced over the entire temperature range studied.

I. Introduction

The macroscopic properties of (dense) dispersions, i.e., both their equilibrium as well as their transport properties, are determined largely by the particle interaction potential and by the average microstructure of the dispersion. For instance, colloidal crystalline structures are observed in dilute systems of latex in water that have been highly deionized. These systems even possess an elastic modulus.[1,2] On the other hand, dilute dispersions of colloidal silica, sterically stabilized by aliphatic chains and dispersed in linear alkanes, form gels that are volume filling.[3] This gelation occurs even at a particle concentration as low as 3% (v/v). Therefore, in both systems there is long-range order, but the origin of the order is different. In the colloidal crystal the structure formation is caused by long-range repulsion. The gel formation is brought about by an attraction between the particles; this type of attraction occurs in many everyday systems which are weakly flocculated, such as yogurt and paint. These two examples demonstrate the influence of the (pair) potential on the (micro) structure of the colloidal dispersion.

A colloidal system can be considered as a supramolecular fluid[4,5] of particles in a continuous background. With this approach the statistical mechanical theories developed for simple fluids can be used to describe the equilibrium properties and structures. The microstructure is described with the pair distribution function, which gives the probability of finding another particle at a center-to-center distance r from a central particle. The Fourier transform of the pair distribution function gives the experimentally accessible function called the structure factor, $S(K)$, where K is the length of the wave vector. One particular theory and description, the so-called hard-sphere theory, is well developed and is used very often. In this theory and in the computer simulations based on this model, the spherical particles interact only at closest approach through an infinitely high repulsive potential. Thus there is only an excluded volume effect. Since equal spheres exclude a volume 4 times their own volume, the second virial coefficient in such a system has the value of $4V_{HS}$,

where V_{HS} is the volume of a hard sphere. The hard-sphere approach is also highly successful[6,7] in systems where the potential rises more gradually, as does, for instance, a Yukawa type potential. In those cases one adjusts (at each density) the effective hard-sphere radius or equivalently the hard-sphere volume fraction. With this adjusted density, the equilibrium structure and thermodynamic properties can be calculated reliably from the hard-sphere model.

A completely different situation arises when the steeply repulsive part of the particle potential is preceded by an attractive part. The potential can be described by a square well or by a more triangular form such as a Lennard-Jones potential. This distinction introduces only slight quantitative differences in our situation. Qualitatively one can say that the distance at closest approach is still governed by the ("physical") steeply repulsive part of the potential. Therefore, at medium to high densities the structure factor will not change very much, except for $K \rightarrow 0$. The value of $S(K=0)$ is equal to the isothermal (osmotic) compressibility of the system. For sufficiently strong attractions, the system will show a phase transition of the gas–liquid type. Therefore, the compressibility must go to high or even infinite values when the spinodal line is passed. This behavior is indeed observed for colloidal systems. For instance, De Hek and Vrij,[8] Vincent et al.,[9] and Sperry et al.[10] describe so-called depletion flocculation experiments. Adding polymer molecules to an otherwise stable dispersion gives rise to an effective attraction between the particles. The systems described by Jansen et al.[11] and Edwards et al.[12] consist of sterically stabilized colloidal par-

† Van't Hoff Laboratory.
‡ University of Twente, Chemical Physics Lab, P.O. Box 217, 7500 AE Enschede, The Netherlands.
§ Institut Laue Langevin, BP156X, F-3804, Grenoble, Cedex, France.

(1) Dubois Violette, E.; Pieranski, P.; Rothen, F.; Strzelecki, L. *J. Phys. (Les Ulis, Fr.)* 1980, *41*, 360.
(2) Ackerson, B. J.; Clarke, N. A. *Physica (A) Amsterdam* 1983, *118*, 221.
(3) Rouw, P. W.; Vrij, A.; de Kruif, C. G. *Colloids Surf.* 1988, *31*, 299.
(4) Perrin, J. *Compt. Rend.* 1914, *158*, 1168.
(5) *Physics of complex and supramolecular fluids*; Safran, S. A., Clarke, N. A., Eds.; Wiley: New York, 1987.
(6) Hayter, J. B.; Hansen, J. P. Institut Laue Langevin, Report 82H-A14T, 1982.
(7) Nieuwenhuis, E. A.; Pathmamanoharan, C.; Vrij, A. *J. Colloid Interface Sci.* 1981, *81*, 196.
(8) de Hek, H.; Vrij, A. *J. Colloid Interface Sci.* 1981, *84*, 409.
(9) Vincent, B.; Luckham, P. F.; Waite, F. A. *J. Colloid Interface Sci.* 1980, *73*, 508.
(10) Sperry, P. R.; Hopfenberg, H. B.; Thomas, N. L. *J. Colloid Interface Sci.* 1982, *82*, 62.
(11) Jansen, J. W.; de Kruif, C. G.; Vrij, A. *J. Colloid Interface Sci.* 1986, *114*, 471, 481, 492, 501.

ticles dispersed in a marginal solvent. In these systems the effective attraction is thought to originate from the difference between the interaction of solvent with chain and chain with chain. The same system was recently used by Rouw and de Kruif[13] to study the behavior of the collective diffusion coefficient in an adhesive hard-sphere dispersion. They found that a square well pair potential of varying depth (depth varying with temperature) is adequate for describing the reduced diffusion in an adhesive hard-sphere system.
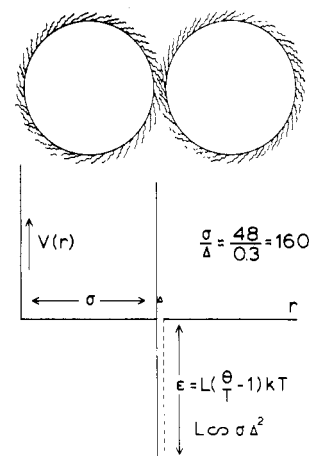
By designing special algorithms, Seaton and Glandt,[14,15] and independently Kranendonk and Frenkel,[16] were able to do Monte Carlo (MC) computer simulations on adhesive hard-sphere systems. Results compare favorably in most respects with the theory developed by Baxter[17] for adhesive hard spheres. The theory and the MC simulations give among other things the compressibility and the "structure" of the system as a function of the stickiness parameter τ.

In this study we will compare Baxter's theory with experimental neutron-scattering data on the structure factor and compressibility of adhesive hard spheres. We used dispersions of sterically stabilized silica in benzene. In good solvents (e.g., cyclohexane) these particles were shown to behave like hard spheres.[18-20] In marginal solvents like benzene, the interaction can be described as being of the hard-sphere type at high temperatures, whereas at lower temperatures an attraction occurs.[3]

This paper is organized as follows. In section II we give the relevant equations and connect the interaction model we use for our adhesive spheres with Baxter's model. After describing the experiments in section III we discuss the obtained results and compare them with theory in section IV.

II. Theory

Pair Potential of Sterically Stabilized Silica Particles. The stabilization of colloidal dispersions against flocculation as a result of the adsorption or grafting of polymer chains onto the particle surfaces is described by Napper[21] and Hesselink, Vrij, and Overbeek.[22] From calculations on the dispersion forces between the particles we find that even a thin layer of different material reduces to negligible values the contribution that the cores make to the dispersion forces. In other words, the interaction of the surface (polymeric) layer either with solvent molecules or with a layer of neighboring particles is dominant. In addition to this enthalpic contribution to the chain-chain and chain–solvent interaction, we also take entropic effects into account. We do this by applying a relation that is similar to the Flory–Huggins expression.[3] In this study we work with silica particles onto whose surfaces octadecyl chains are grafted. A schematic drawing is given in Figure 1. Although the chains are only 18 carbon atoms long,

(12) Edwards, J.; Everett, D. H.; O'Sullivan, T.; Pengalon, I.; Vincent, B. *J. Chem. Soc., Faraday Trans. 1* **1984**, *80*, 2599.
(13) Rouw, P. W.; de Kruif, C. G. *J. Chem. Phys.* **1988**, *88*, 7799.
(14) Seaton, N. A.; Glandt, E. D. *J. Chem. Phys.* **1987**, *86*, 4668.
(15) Seaton, N. A.; Glandt, E. D. *J. Chem. Phys.* **1987**, *87*, 1785.
(16) Kranendonk, W. G. T.; Frenkel, D. *Mol. Phys.* **1988**, *64*, 403.
(17) Baxter, R. J. *J. Chem. Phys.* **1968**, *49*, 2770.
(18) de Kruif, C. G.; Jansen, J. W.; Vrij, A. In *Physics of complex and supramolecular fluids*; Safran, S. A., Clarke, N. A., Eds.; Wiley: New York, 1987.
(19) de Kruif, C. G.; Briels, W. J.; May, R. P.; Vrij, A. *Langmuir* **1988**, *4*, 668.
(20) Vrij, A.; Jansen, J. W.; Dhont, J. K. G.; Pathmamanoharan, C.; Kops-Werkhoven, M. M.; Fijnaut, H. M. *Faraday Discuss. Chem. Soc.* **1983**, *76*, 19.
(21) Napper, D. H. *Polymeric stabilization of colloidal dispersions*; Academic Press: London, 1983.
(22) Hesselink, F. Th.; Vrij, A.; Overbeek, J. Th. G. *J. Phys. Chem.* **1971**, *75*, 2094.

Figure 1. Schematic drawing of two colloidal silica particles covered with a layer of octadecyl chains.

we still model the interaction as in polymer physics. Since the chains are bound to the surface of the particles, the θ temperature of the chain solvent pair is different from that of the free chain solvent pair. Below the θ temperature the particles are effectively attractive. We describe the potential by a square well, the width of which equals Δ. The depth of the well is given by

$$\epsilon = L(\theta/T - 1)kT \tag{1}$$

where L is an adjustable parameter proportional to the overlap volume of the stabilizing layers. Thus

$$L \sim \Delta^2\sigma$$

where σ is the hard-core particle diameter and Δ is the length of interpenetration of the stabilizing chains. The maximum value of Δ is the thickness of the stabilizing layer. From SANS measurements[19] it follows that this thickness is ~ 1.8 nm. From elemental analysis it follows that the surface is effectively close packed with chains, and therefore a nematic-like layer probably forms on the surface. Although the value of Δ is not known exactly, it is clear and essential for what follows that the ratio σ/Δ is large. A reasonable value for Δ obtained from different experiments appears to be 0.3 nm. With a typical particle diameter of 48 nm, the ratio $\sigma/\Delta = 160$.

Given this pair potential it is now possible to calculate thermodynamic and structural properties of such a dispersion. The second virial coefficient is calculated from

$$B_2 = 2\pi \int_0^\infty (1 - \exp(-V(r)/kT))r^2 \, dr \tag{2}$$

The reciprocal structure factor at $K = 0$ is given by the inverse osmotic compressibility

$$S^{-1}(K=0) = (kT)^{-1}[\delta\rho/\delta\Pi]_T^{-1} = 1 + 2B_2\phi + \vartheta(\phi^2) \tag{3}$$

By measuring $S(K=0)$ as a function of volume fraction ϕ at each temperature, one can determine the temperature dependence of B_2. When attractions are sufficiently strong, the system will show a phase transition of the gas–liquid type. From the condition $\delta\Pi/\delta\phi = 0$ it follows that $S^{-1}(K=0) = 0$, and at the spinodal temperature $B_2 = (-2\phi)^{-1}$. Therefore, for a 5% (v/v) dispersion B_2 may vary from 4 (for hard spheres) to -10 before a spinodal decomposition sets in. The osmotic compressibility can be determined by extrapolating the measured structure factor $S(K)$ to zero wave vector.

The normalized scattering intensity in a neutron (or a light) scattering experiment is given by

$$R(K) = V_p(\rho_p - \rho_s)^2\phi P(K) \, S(K) \tag{4}$$

where V_p is the volume per particle, ρ is the scattering length density of particles (and solvent), ϕ is the volume fraction, and $P(K)$ is the intraparticle interference factor. $S(K)$ is the above-mentioned structure factor accounting for interparticle interferences. For a polydisperse system this separation is not unique, but one can define an experimental structure factor by

$$S(K) = \frac{\phi_0 R(K,\phi)}{\phi R(K,\phi_0)} \qquad (5)$$

where ϕ_0 is a low volume fraction for which $S(K) = 1$ at all K. For (polydisperse) hard spheres, $S(K)$ can be calculated in the so-called Percus–Yevick approximation. For other types of pair potentials, different approximations are made. A solution of the Percus–Yevick equation for an adhesive pair potential was obtained by Baxter.[17]

Baxter's Adhesive Hard-Sphere Potential. Baxter defined a pair potential by

$$
\begin{aligned}
V(r)/kT &= +\infty & 0 < r < \sigma \\
&= \ln\left[12\tau\Delta/(\sigma + \Delta)\right] & \sigma \le r \le \sigma + \Delta \\
&= 0 & \sigma + \Delta < r
\end{aligned}
$$

Here τ is a measure of the stickiness and can be considered as a (reduced) temperature. After all thermodynamic quantities are calculated, the limit for $\Delta \to 0$ is taken.

It has been shown by Kranendonk and Frenkel[16] that Baxter's solution for the Ornstein–Zernike equation in the Percus–Yevick approximation correctly predicts the essential features of a sticky hard-sphere system.

In order to relate the parameters in both models, we compare the resulting expressions for the second virial coefficient. Measurements essentially provide this quantity. In Baxter's approach B_2 is given by

$$B_2/V_{HS} = 4 - 1/\tau$$

Integrating our square well potential gives

$$B_2/V_{HS} = 4 - 12(\Delta/\sigma)[\exp(L(\theta/T - 1)) - 1] \qquad (6)$$

Baxter's τ parameter is calculated from

$$1/\tau = 12(\Delta/\sigma)[\exp(L(\theta/T - 1)) - 1] \qquad (7)$$

which equals the γ parameter used by Jansen.[11] Batchelor[23] and Rouw et al.[24] used an α parameter where $\alpha = 2\gamma = 2/\tau$. Rewriting eq 7 results in

$$\ln(1 + \sigma/12\Delta\tau) = -L + L\theta/T \qquad (8)$$

So from the measurement of τ as a function of temperature one can determine L and θ.

To use the above approach one needs to find the osmotic second virial coefficient, and the technique is probably only successful for dilute dispersions since for higher densities higher virial coefficients play a role as well.

The theory as developed by Baxter permits yet another approach. The Fourier transform of the direct correlation function can be used to calculate $S(K,\phi,\tau)$. The relevant equations can be found in Baxter's paper.[17] The idea is to make use of all information contained in the experimentally determined structure factor that is related to the Fourier transform of the direct correlation function, $\tilde{c}(K)$, through

$$\tilde{c}(K) = (S(K) - 1)/(nS(K)) \qquad (9)$$

where n is the number density of the particles. Developing the Fourier transform of $c(r)$ in series leads to

$$\tilde{c}(K) = A + BK^2 + \vartheta(K^4)$$

where

$$A = \tilde{c}(K=0) = 4\pi \int_0^\infty c(r)r^2 \, dr$$

$$B = -2\pi/3 \int_0^\infty c(r)r^4 \, dr$$

The direct correlation function $C(r) = rc(r)$ is given by Baxter (ref 17, eq 11) in terms of potential parameters and particle density. Performing the integration leads to the following set of equations:

$$A/v_0 = -8\alpha - 6\beta + 2\lambda - \phi(2\alpha + \lambda^2) \qquad (10)$$

$$B/v_0 = \sigma^2(4\alpha/5 + 2\beta/3 - \lambda/3 + \phi\alpha/4 + \phi\lambda^2/12) \qquad (11)$$

The functions α and β are quadratic in λ and are given by (ref 17, eq 17 and 18)

$$\alpha = \frac{(1 + (2 - \lambda)\phi + \lambda\phi^2)^2}{(1 - \phi)^4}$$

$$\beta = [-3\phi(2 + \phi)^2 + \lambda\phi(2 - 2\phi) \times (1 + 7\phi + \phi^2) - \lambda^2\phi^2(1 - \phi)^2(2 + \phi)]/[2(1 - \phi)^4]$$

where $v_0 = \pi\sigma^3/6$. Finally, the interaction parameter λ is given as a function of τ and ϕ by (ref 17, eq 21)

$$\tau = [(1 + \phi/2)/(1 - \phi)^2]\lambda^{-1} - [\phi/(1 - \phi)] + \phi\lambda/12 \qquad (12)$$

In Figure 2 we plot A/v_0, B/v_0, and τ as a function of λ for a series of volume fractions pertinent to the experiments described later. From the experimental structure factor we calculated $\tilde{c}(K)$. We plotted $\tilde{c}(K)$ against K^2 at each ϕ and temperature. Fitting these data at small K to a linear equation gives A and B. Then we read from parts a and b of Figure 2 the value of λ and from Figure 2c the value of τ. Ideally τ is independent of volume fraction. The two independent values of τ, one value from the slope and one from the ordinate, should be equal if the applied model is appropriate for the experimental results at hand.

Polydispersity is an important aspect of the problem, but it is not dealt with in this paper. There is a solution of the Percus–Yevick equation for polydisperse hard spheres,[25,26] but we are not aware of an expression for the structure factor for polydisperse adhesive hard spheres. Another complicating factor may be that the stickiness of the spheres may vary, not only because of size polydispersity but also because of topology of the surface. Previous experiments, however, have shown that many of these effects are absorbed in the adjustable parameters.

III. Experimental Section

Sample Characterization. The silica system, denoted by SP23 and dispersed in cyclohexane, used in previous SANS experiments[19] and for rheological measurements[27] was dried under a mild nitrogen flow at 70 °C. Weighed amounts of the dry silica were dispersed in weighed amounts of benzene at 50 °C. The specific volume of SP23 is taken as 0.63 $cm^3\cdot g^{-1}$, and the density of benzene is taken as 0.87 $cm^3\cdot g^{-1}$. With this we calculated volume fractions ϕ as given in Table I. The samples were stored at 50 °C to prevent phase separation. From the sample tube with $\phi = 0.096$ we took a sample to determine the cloud point temperature. The cloud point is found from the sharp increase in turbidity when the sample reaches the phase separation temperature. We also determined the diffusion coefficient of SP23 dispersed in benzene by dynamic light scattering as a function of temperature. For details see ref 13. Static light-scattering intensities were measured in a SOFICA setup. The three ex-
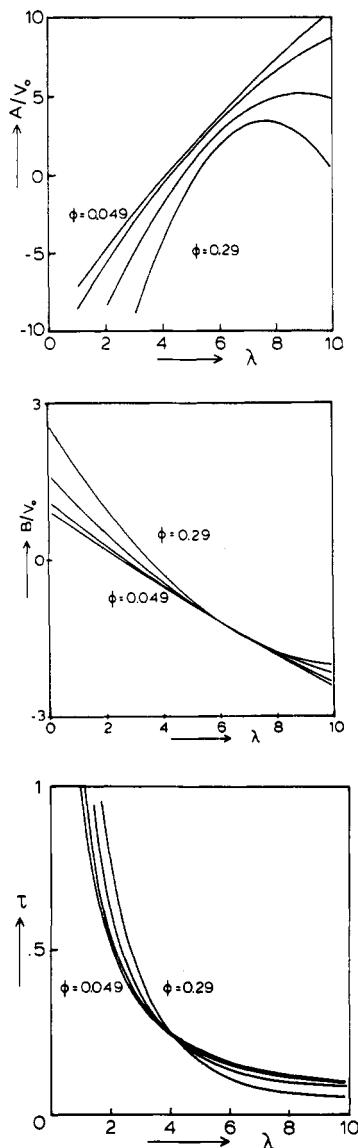
(23) Batchelor, G. K. *J. Fluid Mech.* **1972**, *52*, 245.
(24) Rouw, P. W.; Vrij, A.; de Kruif, C. G. *Progr. Colloid Polym. Sci.* **1988**, *76*, 1.

(25) Vrij, A. *J. Chem. Phys.* **1978**, *69*, 7742.
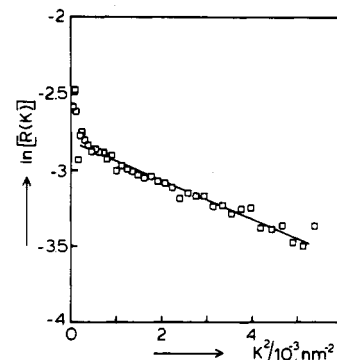(26) Vrij, A. *J. Chem. Phys.* **1979**, *71*, 3267.
(27) van der Werff, J. C.; de Kruif, C. G. *J. Rheol. (N.Y.)*, in press.

Figure 2. (a, Top) Plot of A/V_0 against λ. (b, Middle) Plot of B/V_0 against λ. (c, Bottom) Plot of τ against λ. Volume fractions are 0.049, 0.096, 0.19, and 0.29.

Figure 3. Guinier plot of scattering of silica particles in benzene. The data are obtained by averaging the results of measurements at 40.1, 38.1, 35.7, 35.0, and 34.4 °C. The slope corresponds to an optical radius of 25.3 nm.

perimental results mentioned above gave us reliable data concerning the phase separation behavior of the colloidal system. From these data we calculated approximate values of the θ temperature and the interaction parameter L. Using these values to calculate the temperature dependence of B_2, we could also calculate model structure factors according to Baxter's theory. On the basis of these model calculations we chose a series of temperatures at which to perform the SANS measurements.

SANS Measurements. Use was made of the D11 spectrometer of the Institut Laue-Langevin at Grenoble (France) where we were allocated 24 h of beam time. In view of the predictions of Baxter's theory, the detector was placed near the maximum distance from the sample, i.e., at 36.5 m. The end of the neutron guide ("collimation length") was set to 40.5 m. Although with sample path lengths of 1 mm, slight multiple scattering may occur, we nevertheless used this path length so as to obtain sufficient scattering into the detector. We assume that the possible contribution of multiple scattering to the scattering pattern can be neglected, in this case for several reasons. Multiple scattering is primarily seen in parts of the scattering curve where the intensity is low and which are close to higher intensities. So minima, for instance, in the particle structure factors are washed out. We showed that this effect is only slightly present with path lengths of 0.5 mm and is absent at 0.2 mm. In the present study we have very flat scattering curves, the K dependence of which is insensitive to multiple scattering. Multiple scattering may influence the intensity level of the scattering curves. For a detailed dis-

cussion of the instrument D11 we refer to the thesis of Harris[28] and to ref 29 and 30.

Sample Rack and Temperature Control. Temperature control of the samples is of extreme importance, as could be seen from model calculations. Since the usual sample racks available at D11 are not well suited for temperature control, we decided to construct a new rack in our laboratory. This rack has 10 cell positions. Both types of cuvette (type 121 and type 120 with special 1-mm quartz cells) as produced by Hellma fit in the rack. Temperature is measured at positions 3 and 8 with a platinum resistor. Temperature could be kept within 0.1 °C in the range 0–50 °C by using a thermostatically controlled water bath. The rack is now available at Grenoble.

Data Reduction. The scattered intensities were averaged radially. Corrections were made for background, noise, transmission, and empty cell. Finally, the data were scaled to absolute intensities and corrected for detector sensitivity; as a reference we used the scattering of pure water at a shorter sample–detector distance (<36.5 m). The contribution of incoherent scattering can be neglected at a 36.5-m detector distance. The necessary equations are given in ref 28 and 19. The data were treated by standard computer programs at the ILL, stored on tape, and further processed on our laboratory computer.

IV. Results and Discussion

Form Factor. In previous experiments we showed that for our silica system the shape of the scattering curves up to volume fractions $\phi = 0.02$ is insensitive to (hard sphere) structure effects for our silica system. Ideally this will hold also for sticky hard spheres. In Figure 3 we plotted the average scattering intensities at different temperatures for the sample with $\phi = 0.019$. More detailed plots of the data showed that there is no systematic temperature dependence of the scattering intensity. We therefore averaged all those files to one file. The slight upward curvature at small K values is attributed to the presence of a few doublets/multiplets in the dispersion. Leaving out the first four data points at low K, we fitted the data to a Guinier plot $I(K) = I(0) \exp(-K^2 R_g^2/3)$. The slope of a plot of ln $(I(K))$ vs K^2 lets us obtain the radius of gyration R_g (Figure 3). We found $R_g = 19.6 \pm 1$ nm. In the previous study,[19] where the same particles were dispersed in a good solvent (cyclohexane), we found $R_g = 20.3 \pm 0.3$ nm. In that study, measurements were made over a large K range. By fitting the full $P(K)$, we found $a_{core} = 22.5$ nm. Assuming a log-normal distribution, the standard deviation was found to be 0.12. Since the steric layer on the particles is invisible, we added 1.8 nm in order to find the hard-sphere inter-

(28) Harris, N. *Small Angle Neutron Scattering from Colloidal Systems*; Ph.D. Thesis, Oxford, 1980.
(29) Ibel, K. *J. Appl. Crystallogr.* **1976**, *9*, 296.
(30) Neutron Research Facilities at the ILL high flux reactor; Institut Max von Laue–Paul Langevin, 1980.

Table I. Results of SANS Measurements on SP23 Dispersed in Benzene

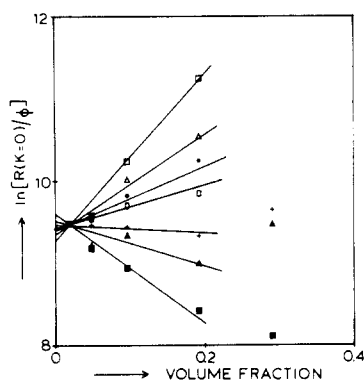| T, °C	$-2B_2$, cm³ g⁻¹	ϕ	A/V_0	B/V_0	τ_A	τ_B	τ_0
52.0	−7	0.049	−7.41	0.641	0.85	0.82	0.80
		0.096	−7.06	0.637	0.85	0.85	
		0.19	−8.31	0.51	0.62	0.58	
		0.29	−8.36	0.35	0.41	0.40	
40.1	−2	0.049	−4.71	0.317	0.35	0.59	0.47
		0.096	−2.55	−0.029	0.32	0.38	
		0.19	−3.08	−0.07	0.36	0.35	
		0.29	−0.49	−0.68	0.14	0.17	
38.1	−1	0.049	−2.62	0.128	0.36	0.47	0.40
		0.096	−1.21	−0.207	0.27	0.32	
		0.19	−1.21	−0.44	0.23	0.25	
		0.29	1.49	−1.15	0.12	0.12	
36.4	2	0.049	−0.38	−0.37	0.26	0.27	0.30
		0.096	0.95	−0.61	0.24	0.23	
		0.19	0.73	−0.77	0.18	0.19	
		0.29	3.13	−1.81	0.09	0.10	
35.7	4	0.049	−0.37	−0.30	0.26	0.30	0.29
		0.096	1.75	−0.75	0.18	0.20	
		0.19	1.62	−0.98	0.16	0.18	
		0.29	2.36	−1.60	0.11	0.08	
35.0	6	0.049	1.01	−0.55	0.22	0.24	0.26
		0.096	3.07	−1.01	0.16	0.17	
		0.19	2.60	−1.20	0.14	0.15	
		0.29	2.62	−2.54	0.10		
34.4	9	0.049	1.75	−0.60	0.20	0.23	0.24
		0.096	3.91	−1.07	0.14	0.16	
		0.19	3.31	−1.31	0.13	0.14	
		0.29	3.22	−5.80	0.09		
32.6		0.049	6.27	−1.60	0.14	0.14	0.20
		0.096	3.32	−1.56	0.15	0.15	
		0.19					
		0.29					

Figure 4. ln $(I(K=0)/\phi)$ against ϕ. The initial slope of these plots represents $2B_2$. ■, 52.0; ▲, 40.1; +, 38.1; O, 36.4; ★, 35.7; △, 35.0; □, 34.4 °C.

Figure 5. Representative plot of $\tilde{c}^*(K) = \tilde{c}(K)/V_0$ against K^2 for $\phi = 0.096$ and $T = 40.1$ °C (+) and 35.7 °C (o).

action diameter. The diameter of the particles is thus given by $\sigma = 2(22.5 + 1.8) = 48.6$ nm.

Compressibility. At higher volume fractions the scattered intensity is proportional to the structure factor, $S(K)$, as well. In order to find $S(K=0)$, we made plots of ln $(S(K))$ vs K^2. The initial slope of $1/S(K=0)$ vs ϕ is $2B_2$ (see eq 3). Our data do not allow such a procedure since volume fractions should not exceed 5%. However, for hard spheres it is an empirical finding[31] that a plot of ln $(S(K=0))$ vs ϕ is virtually linear over the whole volume fraction range with a slope $\approx 2B_2$. For adhesive hard spheres it follows from Baxter's theory that the linear dependence of ln $[S(K=0)]$ on ϕ only holds for high values of τ ($\tau \geq 1$). For smaller values of τ the linear relation is restricted to small values of ϕ. Nevertheless, in Figure 4 we plotted ln $(R(K=0)/\phi)$ vs volume fraction for each temperature. Since the scattering of the lowest volume fraction sample is (taken) independent of the temperature, we assumed
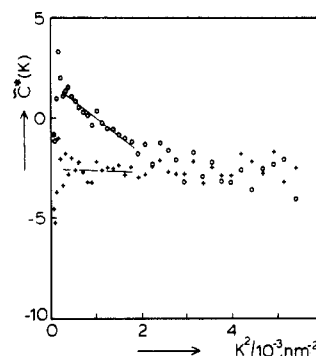
that $S(K=0) = 1$ for this sample. Therefore, all straight lines drawn in Figure 4 pivot around this first point. It is clearly visible that at high temperatures the slope is negative, corresponding to a positive B_2, whereas at low temperatures B_2 is strongly negative. The lines are drawn giving the low volume fraction data an increased weight. The slopes, i.e., B_2, are given in Table I. B_2 values determined in this way should only be treated in a qualitative way since they are based on a small number of data.

λ and τ Parameters. In Figure 5 we have drawn representative plots of $\tilde{c}^*(K) = \tilde{c}(K)/V_0$ against K^2 for $\phi = 0.096$ at two temperatures. After omission of the first few points the initial part of the plot was fitted to a linear equation. The slope and ordinate are given in Table I. From plots such as Figure 2 we read λ and τ values also given in Table I. From studying these data we conclude that, considering the error ranges, there is no really systematic difference between values of τ obtained from slope and intercept. It appears that τ depends on volume fraction. In fact we could have treated both volume fraction and τ as independently adjustable parameters in Baxter's theory, but this would have led to very unrealistic

(31) Frenkel, D.; Vos, R. J.; de Kruif, C. G.; Vrij, A. *J. Chem. Phys.* **1986**, *4*, 4625.
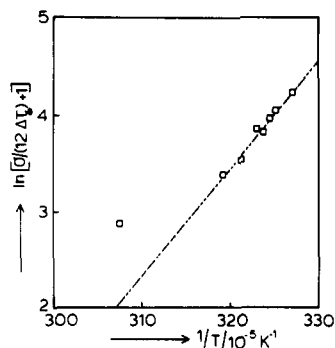
Figure 6. ln $(1 + \sigma/12\Delta\tau)$ vs $1/T$ according to eq 8.
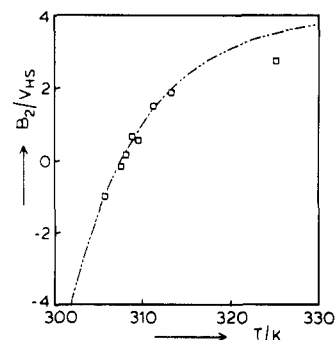
Figure 7. Experimental and calculated temperature dependence of the second virial coefficient B_2. Squares are obtained from extrapolating τ values to zero volume fraction.

values of ϕ. So we notice an important difference between experiment and theory, i.e., that the τ-parameter is ϕ dependent. A review of our data shows that Baxter's temperature τ can be represented as

$$\tau(T) = \tau_0(T) - 0.7\phi$$

The volume fraction dependence is weak and would not have been noticed if we had restricted our experiments to $\phi < 0.2$. It is not clear where this ϕ dependence originates. Qualitatively it means that at constant temperature attraction increases with increasing volume fraction.

Plotting a line with slope = -0.7 through the experimental data, we found $\tau_0(T)$ as given in the third column of Table I. In Figure 6 we plot $\tau_0(T)$ according to eq 8 using $\sigma = 48.6$ nm and $\Delta = 0.3$ nm. A least-squares fit (excluding the first point) gives $L = 32 \pm 2$ and $\theta = 346 \pm 17$ K. These values can be used to calculate B_2 from

$$B_2 = 4 - 12(\Delta/\sigma)[\exp(L(\theta/T - 1)) - 1]$$

In Figure 7 we plot this function together with experimental points defined as $B_2 = 4 - 1/\tau_0$. Since τ values were extrapolated to $\phi = 0$, these B_2 values are the true second virial coefficients of the osmotic pressure. These τ values account for the particle pair interaction as a function of temperature. In ref 24 we report on turbidity and dynamic light-scattering experiments on the same system as used here. Measurements were made at relatively low volume fractions. The turbidity results can indeed be described very adequately by the values $L = 32$ and $\theta = 346$ K.

Structure Factors. In Figures 8–11 the experimental results are plotted together with the calculated structure factors. Theoretical curves were obtained by using a Fortran computer program called SSPHERES.[32] For each temperature and volume fraction, τ was evaluated from $\tau = \tau_0 - 0.7\phi$. We comment on our results as follows.

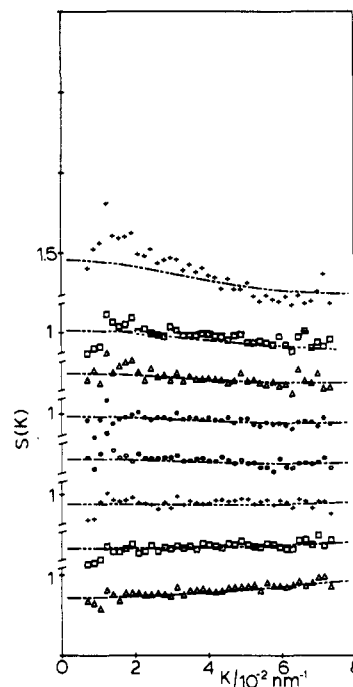(32) Fortran computer program SSPHERES, courtesy of Winfried Kranendonk.

Figure 8. Structure factor against momentum transfer, $\phi = 0.049$. $\triangle$, 52.0; $\square$, 40.1; +, 38.1; O, 36.4; $\star$, 35.7; $\triangle$, 35.0; $\square$, 34.4; +, 32.6 °C. The drawn lines are calculated; see text.
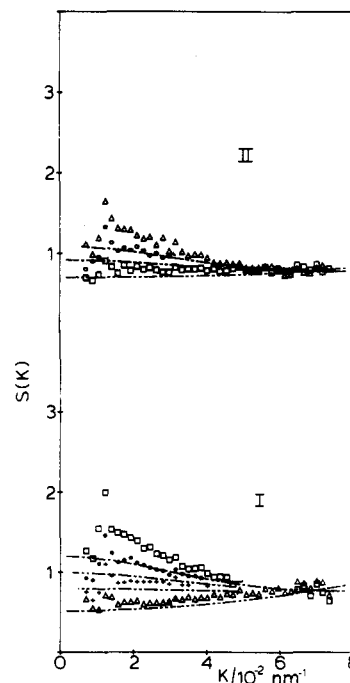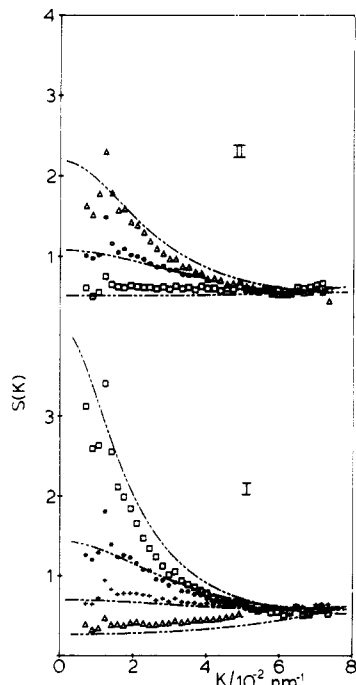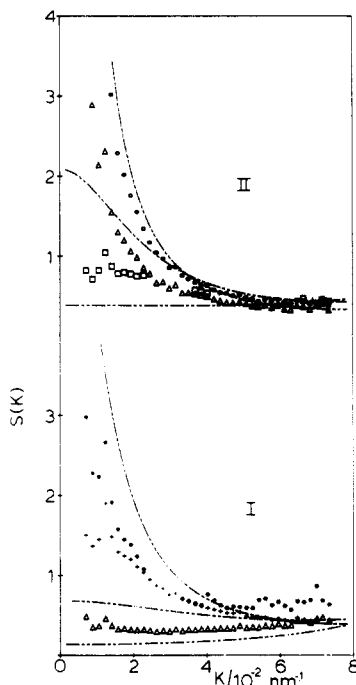
Figure 9. Structure factor against momentum transfer, $\phi = 0.096$. We divided the data into two sets of temperatures for clarity. Set I: $\triangle$, 52.0; +, 38.1; $\star$, 35.7; $\square$, 34.4 °C. Set II: $\square$, 40.1; O, 36.4; $\triangle$, 35.0 °C. The drawn lines are calculated, see text.

All experimental data points and the calculated curves cross over between $K = 0.05$ and 0.07 nm^{-1}. This means that in this K region the structure factor is insensitive to the value of τ. We used this feature to calibrate the data on the calculated $S(K)$ values. In order to do this we divided the experimental structure factor by 1.10. The majority of the curves run practically horizontal, and so this division only brings about a small shift and does not change essential features. In fact, the correction is completely justified in the treatment of polydispersity effects in hard-sphere systems, where the division would indicate a polydispersity of 10%. Furthermore, if we take into

Figure 10. Structure factor against momentum transfer, ϕ = 0.19. We divided the data into two sets of temperatures for clarity. Set I: △, 52.0; +, 38.1; ★, 35.7; □, 34.4 °C. Set II: ▢, 40.1; ○, 36.4; △, 35.0 °C. The drawn lines are calculated, see text.

Figure 11. Structure factor against momentum transfer, ϕ = 0.29. We divided the data into two sets of temperatures for clarity. Set I: △, 52.0; +, 38.1; ★, 35.7 °C. Set II: □, 40.1; ○, 36.4; △, 35.0 °C. The drawn lines are calculated, see text.

account that all experimental uncertainties (e.g., multiple scattering, incoherent background, transmission, volume fractions, cell thickness, etc.) accumulate in $S(K)$, this 10% shift is of the same order as these uncertainties together.

As a whole, the experimental data are reproduced very satisfactorily, especially at ϕ = 0.19. This is probably because scattering data are the most accurate for this sample. First of all, temperature is best defined in the middle of the rack. Furthermore, an average, and thus ϕ-independent, τ parameter would attain the value corresponding to ϕ = 0.2. Conversely all these effects could
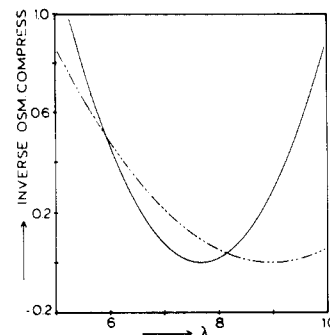
Figure 12. Inverse osmotic compressibility as a function of λ for ϕ = 0.19 (dashed line) and ϕ = 0.29 (solid line).

and do explain why there are small discrepancies. Especially at lower temperatures, B_2 becomes a strong function of temperature. Therefore, a slight misreading of the temperature, say, by 0.2 °C, will change the curves significantly.

There is a remarkable feature in Figure 11. If the temperature is lowered from 41.0 to 36.4 °C and then to 35.0 °C, the osmotic compressibility rises at first but subsequently decreases.

The inverse osmotic compressibility can be found from Baxter's theory (ref 17, eq 31) and is found to be

$$\frac{1}{kT}\frac{\delta\Pi}{\sigma\rho} = 1 + \phi(8\alpha + 6\beta - 2\lambda) + \phi^2(2\alpha + \lambda^2)$$

In Figure 12 we plot the inverse osmotic compressibility as a function of λ for ϕ = 0.19 and 0.29. At the minimum value of the curves osmotic compressibility is infinite. Values of $\lambda > (1 + 2\phi)/(\phi(1 - \phi))$ have to be discarded since for these values the pair distribution function is unbounded. The limiting values of λ are the minima of the curves shown in Figure 12. At these points the system reaches a spinodal. Therefore, Baxter's theory predicts that osmotic compressibility will increase monotonically with temperature to the spinodal line. For the values of λ that have to be discarded the system is in the two-phase region, and phase separation is expected to occur.

From Figure 12 and 2c we determined the spinodal values of τ. Using the values of L, θ, Δ, σ, and ϕ we calculate τ for T = 35.0 °C. For ϕ = 0.29 we found τ to be smaller than the spinodal value. Therefore, for this situation concentration fluctuations will occur that move the system toward the binodal line, thus decreasing osmotic compressibility. Although during the 15 min or so which the experiment takes no appreciable phase separation occurred, we think that the decrease in osmotic compressibility for the sample mentioned above is due to the fact that the system was in the two-phase region. This observation thus sustains the description used.

V. Conclusions

Low-angle structure factor measurements on colloidal silica dispersions allow the evaluation of attractive interaction parameters. The applied square well model in combination with Baxter theory works satisfactorily. At higher densities a slight volume fraction dependence is observed. Experimental data can be reproduced almost quantitatively.

Registry No. Silica, 7631-86-9.